ACVR1^{R206H} FOP mutation alters mechanosensing and tissue stiffness during heterotopic ossification

Julia Haupt[a,b], Alexandra Stanley[a,b], Claire M. McLeod[a,c,d], Brian D. Cosgrove[a,c,d], Andria L. Culbert[a,b], Linda Wang[a,b], Foteini Mourkioti[a,e], Robert L. Mauck[a,c,d,f], and Eileen M. Shore[a,b,g,*]

Departments of [a]Orthopaedic Surgery, [e]Cell and Developmental Biology, and [g]Genetics and [b]Center for Research in FOP and Related Disorders, Perelman School of Medicine, and Departments of [c]Bioengineering and [f]Mechanical Engineering and Applied Mechanics, School of Engineering and Applied Science, University of Pennsylvania, Philadelphia, PA 19104; [d]Translational Musculoskeletal Research Center, Corporal Michael J. Crescenz VA Medical Center, Philadelphia, PA 19104

ABSTRACT **An activating bone morphogenetic proteins (BMP) type I receptor ACVR1 (ACVR1^{R206H}) mutation enhances BMP pathway signaling and causes the rare genetic disorder of heterotopic (extraskeletal) bone formation fibrodysplasia ossificans progressiva. Heterotopic ossification frequently occurs following injury as cells aberrantly differentiate during tissue repair. Biomechanical signals from the tissue microenvironment and cellular responses to these physical cues, such as stiffness and rigidity, are important determinants of cell differentiation and are modulated by BMP signaling. We used an *Acvr1*$^{R206H/+}$ mouse model of injury-induced heterotopic ossification to examine the fibroproliferative tissue preceding heterotopic bone and identified pathologic stiffening at this stage of repair. In response to microenvironment stiffness, in vitro assays showed that *Acvr1*$^{R206H/+}$ cells inappropriately sense their environment, responding to soft substrates with a spread morphology similar to wild-type cells on stiff substrates and to cells undergoing osteoblastogenesis. Increased activation of RhoA and its downstream effectors demonstrated increased mechanosignaling. Nuclear localization of the pro-osteoblastic factor RUNX2 on soft and stiff substrates suggests a predisposition to this cell fate. Our data support that increased BMP signaling in *Acvr1*$^{R206H/+}$ cells alters the tissue microenvironment and results in misinterpretation of the tissue microenvironment through altered sensitivity to mechanical stimuli that lowers the threshold for commitment to chondro/osteogenic lineages.**

Monitoring Editor
Dennis Discher
University of Pennsylvania

Received: Jul 16, 2018
Revised: Oct 17, 2018
Accepted: Oct 25, 2018

This article was published online ahead of print in MBoC in Press (http://www.molbiolcell.org/cgi/doi/10.1091/mbc.E18-05-0311) on October 31, 2018.

The authors declare no competing conflicts of interest with the work presented.

Author contributions: J.H., R.L.M., and E.M.S. designed the study, analyzed, and interpreted data, and wrote the manuscript. J.H., A.S., C.M.M., B.D.C., and A.L.C. conducted experiments, and acquired, analyzed, and interpreted data. F.M. assisted in interpreting data. L.W. performed experiments and data collection. All authors critically reviewed and edited the manuscript.

*Address correspondence to: Eileen M. Shore (shore@pennmedicine.upenn.edu).

Abbreviations used: ACVR1, Activin A receptor, type 1; BMP, bone morphogenetic protein; ECM, extracellular matrix; FOP, fibrodysplasia ossificans progressiva; HO, heterotopic ossification; MEF, mouse embryonic fibroblast; PA, polyacrylamide; RhoA, ras homologue gene family, member A; ROCK, Rho-associated protein kinase; RUNX2, runt-related transcription factor 2.

© 2019 Haupt *et al.* This article is distributed by The American Society for Cell Biology under license from the author(s). Two months after publication it is available to the public under an Attribution–Noncommercial–Share Alike 3.0 Unported Creative Commons License (http://creativecommons.org/licenses/by-nc-sa/3.0).

"ASCB®," "The American Society for Cell Biology®," and "Molecular Biology of the Cell®" are registered trademarks of The American Society for Cell Biology.

INTRODUCTION

Many cancers, cardiovascular disease, and acute and chronic fibrosis are accompanied by increased extracellular matrix deposition and increased tissue stiffness (Ingber, 2003). Normal physical properties of tissues within the body have great diversity, with stiffness ranging from very soft (brain, fat tissue) to rigid (bone) (Cox and Erler, 2011). Cells interpret their environment through force sensing by pulling on surrounding matrix to measure the levels of stiffness and then respond to these physical cues in their tissue microenvironment through activation of mechanosensing signaling pathways. Signals transduced by sensing tissue stiffness impact cell fate decisions by providing instructive differentiation signals. Mechanosensing is regulated and operative during development, leading to diversity in differentiation and organogenesis/morphogenesis, and during postnatal life for maintenance of tissue homeostasis and facilitating regeneration and wound healing

processes (Engler *et al.*, 2006; Georges *et al.*, 2006; Chanet and Martin, 2014). It has been suggested that a mechanosignaling stimulus alone can be sufficient to direct cell differentiation; for example, mesenchymal progenitor cells sensing an environment with the mechanical properties of nascent bone tissue will respond by undergoing osteogenic differentiation (Engler *et al.*, 2006). Recently, it has become widely recognized that altered mechanosensing can also contribute to the pathogenesis of genetic and nongenetic diseases (Ingber, 2003; Dahl *et al.*, 2008; Butcher *et al.*, 2009; Knipe *et al.*, 2015; Kai *et al.*, 2016); however, whether heterotopic ossification (HO), a condition in which extraskeletal bone forms within soft connective tissues (McCarthy and Sundaram, 2005), could be influenced by altered force-sensing and differential interpretation of substrate stiffness remains undetermined.

Fibrodysplasia ossificans progressiva (FOP; MIM #135100) is a rare genetic disease that forms extensive and progressive postnatal ossification within soft tissues (Shore and Kaplan, 2010). The heterotopic bone that forms within soft connective tissues in FOP is normal bone tissue by all evaluated criteria; its aberration lies in the lost regulation of cell fate determination. Mutations in the bone morphogenetic proteins (BMP) type I receptor ACVR1 (Activin A receptor, type 1; alias: ALK2) cause FOP, and all patients with a classic clinical manifestation of the disease possess a recurrent heterozygous c.617G>A (R206H) mutation (Shore *et al.*, 2006; Kaplan *et al.*, 2009). This single-nucleotide substitution results in overactivation of the BMP signaling pathway (Fukuda *et al.*, 2009; Shen *et al.*, 2009; van Dinther *et al.*, 2010; Haupt *et al.*, 2014). The BMP pathway is well established as promoting cartilage and bone formation (Rahman *et al.*, 2015; Salazar *et al.*, 2016), and the ACVR1 R206H mutation has been shown to enhance chondrogenesis and osteogenesis (Shen *et al.*, 2009; van Dinther *et al.*, 2010; Culbert *et al.*, 2014; Haupt *et al.*, 2014). Heterotopic ossification in FOP, as well as in more common nonhereditary HO (Pignolo and Foley, 2005; Shore and Kaplan, 2010), forms through progressive tissue and cellular events that culminate in bone tissue formation within skeletal muscle and other soft connective tissues; these bone-forming lesions are often initiated by tissue damage. In the absence of overt injury, new bone formation in FOP patients occurs spontaneously and episodically, interspersed by apparent periods of quiescence with no HO formation (Kaplan *et al.*, 2008; Shore, 2012). These clinical observations support that factors in addition to the genetic mutation modulate the cellular activity of the mutant receptor to strongly influence disease progression.

Heterotopic ossification in FOP forms through a well-described series of changes within the tissue (Shore and Kaplan, 2010; Chakkalakal *et al.*, 2012; Convente *et al.*, 2018). In response to injury, initial steps of wound healing in FOP tissue appear to be normal, including an early immune response that leads to tissue degradation and removal of damaged tissue. The transition from tissue degradation to regeneration during normal wound healing is a fibroproliferative stage characterized by up-regulated extracellular matrix (ECM) production and remodeling. However, in FOP tissue this trajectory diverges when, instead of repairing and regenerating the injured tissue, progenitor cells aberrantly differentiate to cartilage and bone cells and endochondral bone is formed (Kaplan *et al.*, 1993; Shore and Kaplan, 2010; Culbert *et al.*, 2014; Convente *et al.*, 2018). Alterations in the physical and mechanical properties of the tissue during this stage, and altered sensing of the tissue microenvironment by mutant progenitor cells that are primed to chondro-osseous differentiation by the underlying *ACVR1* mutation, may have major, yet unrecognized, roles in promoting HO by creating a tissue microenvironment that is permissive and/or inductive for chondrogenic and osteogenic differentiation.

In this study, we examined in vivo stiffness and ECM properties of *Acvr1*^{R206H} mutant tissue in response to injury to determine whether the physical/mechanical microenvironment of the tissue where HO forms is altered. Additionally, we determine whether the mutation modulates mechanosensing and mechanosignaling by investigating the ability of cells expressing the FOP mutation to properly sense and respond to the mechanical cues in their microenvironment. Our data support that both changes in the tissue microenvironment and the ability of cells to sense their environment are altered by the FOP *Acvr1*^{R206H} mutation.

RESULTS

Tissue rigidity is increased in fibroproliferative areas following injury of Acvr1$^{R206H/+}$ muscle

Muscle injury frequently triggers heterotopic bone formation in FOP patients, suggesting an aberrant wound healing response in the presence of the *ACVR1*^{R206H} mutation. Expression of *Acvr1*$^{R206H/+}$ in a knock-in mouse model of FOP recapitulates all key clinical features of the disease including HO formation in response to muscle injury (Chakkalakal *et al.*, 2012, 2016; Convente *et al.*, 2018). To investigate changes in skeletal muscle tissue properties in response to injury, we treated *Acvr1*$^{R206H/+}$ knock-in mice with cardiotoxin (Figure 1A). Cardiotoxin (CTX) leads to rapid muscle damage and muscle degradation that is accompanied by an inflammatory response; this catabolic phase is followed by the onset of an anabolic, reconstruction phase characterized by activation of muscle stem cells (e.g., satellite cells) that proliferate, differentiate, and subsequently form new muscle fibers in wild-type tissue (Couteaux *et al.*, 1988; Charge and Rudnicki, 2004; Vignaud *et al.*, 2005; Czerwinska *et al.*, 2012).

To assay lesions in injured muscle from *Acvr1*$^{+/+}$ control littermates and *Acvr1*$^{R206H/+}$ mice at the fibroproliferative stage, animals were killed at days 4 to 5 post–CTX injury (Figure 1A), a time at which no heterotopic bone or cartilage has yet formed (Chakkalakal *et al.*, 2012; Convente *et al.*, 2018), as verified by H&E staining of the injured tissues. Phosphate-buffered saline (PBS) injection in control and mutant mice (Figure 1B) did not induce muscle injury and served as negative controls. Substantial degeneration of muscle tissue was found after CTX injection in both *Acvr1*$^{R206H/+}$ mice and controls. Early stages of wound healing were accompanied by robust fibroproliferation in both mutant and control littermates (Figure 1, B and C). Tissue stiffness was quantified by measuring Young's moduli through atomic force microscopy (AFM) (Levental *et al.*, 2010) of consecutive nonfixed tissue cryosections (Figure 1D, left). Stiffness of healthy uninjured muscle was ~20 kPa, with no significant difference between *Acvr1*$^{R206H/+}$ and control littermates (Figure 1D, right). Fibroproliferative regions in injured areas of control littermates showed a >3.5-fold reduction in rigidity compared with healthy muscle (black columns, Figure 1D, right), consistent with the ongoing turnover of damaged muscular tissue and initial stages of wound healing (Hinz, 2010). Lesions in control littermates were relatively soft (~6 kPa), indicating that these tissues are at an early wound healing (early fibroproliferation) stage, well before the appearance of repaired muscle fibers. However, at the comparable time point, tissue stiffness in fibroproliferative areas of injured *Acvr1*$^{R206H/+}$ tissue was significantly elevated compared with controls, reaching a stiffness of ≥40 kPa, which is ~2-fold higher (Figure 1D, right, red bars) than healthy uninjured muscle, not unlike the pathological stiffening of tissues that is observed in fibrosis or scar tissue (~15–100 kPa) (Liu *et al.*, 2010; Brown *et al.*, 2013) and is a stiffness consistent with previously

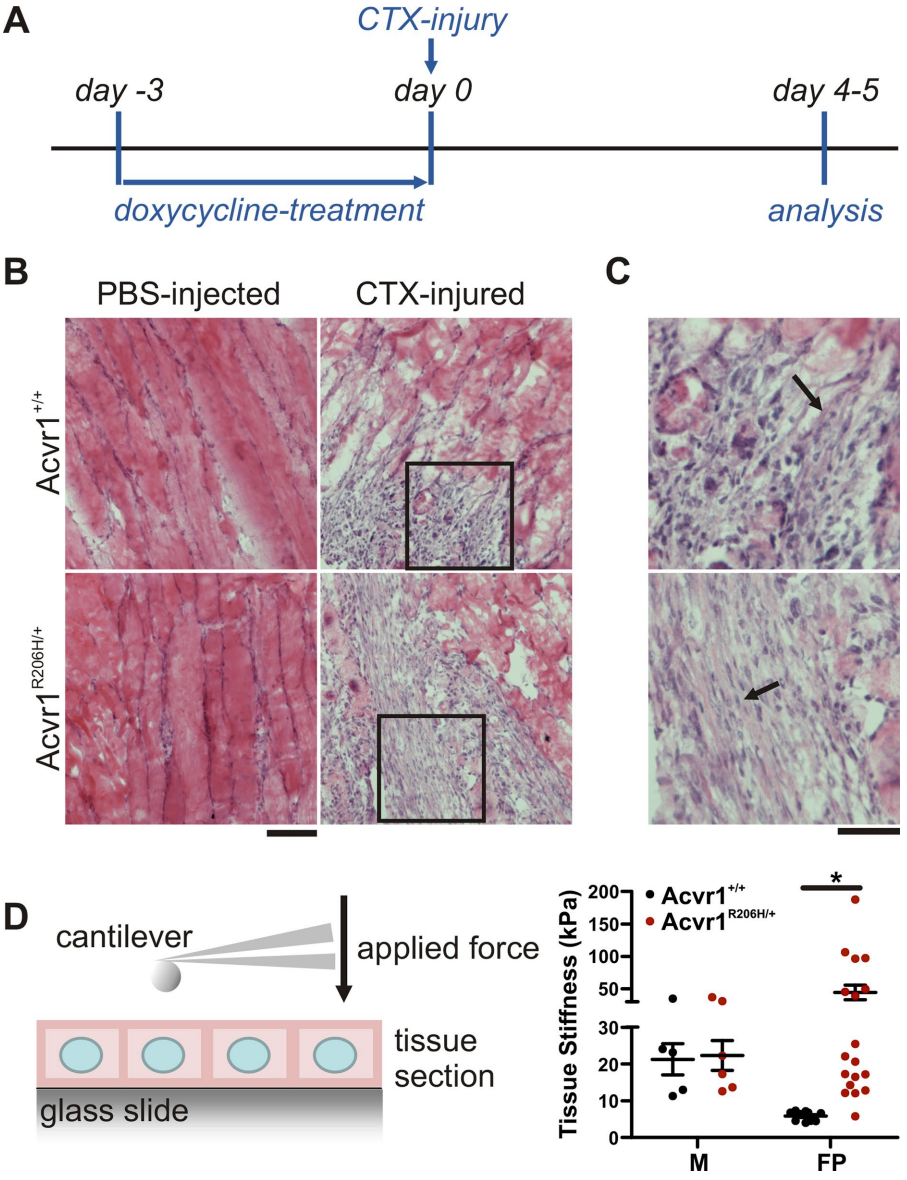

FIGURE 1: Increased fibroproliferative tissue stiffness in response to skeletal muscle injury in *Acvr1*$^{R206H/+}$ mice. (A) Timeline of experimental procedure. The *Acvr1*^{R206H} mutation was expressed in conditional Acvr1$^{R206H/+}$ mice through doxycycline treatment 3 d prior to injection with cardiotoxin or PBS (uninjured control). Littermate controls were treated equivalently. (B) H&E staining of sections from PBS-injected or CTX-injured quadriceps showing areas of healthy muscle and fibroproliferation (arrow) 4 d post–injection of FOP mice or littermate controls. Scale bar represents 100 μm. (C) Enlarged images from insets in B. Scale bar: 50 μm. (D) Tissue stiffness was measured via AFM. Consecutive sections demonstrate increased rigidity of fibroproliferative areas (FP) in FOP lesions compared with healthy muscle (M). Graph represents mean ± SEM for $N = 5–18$ (in M: 5 [control] and 6 [FOP]; in FP: 10 [control] and 18 [FOP]) locations measured across three independently injured limbs. Significance was determined by two-way ANOVA (Bonferroni post test); *$p < 0.05$.

reported AFM measurements of the osteoid microenvironment within bone (Engler *et al.*, 2006). Intact skeletal muscle, located in close proximity to the lesions in the *Acvr1*$^{R206H/+}$ CTX-injected group, also scaled to 20 kPa, supporting that tissue stiffening is locally restricted to fibroproliferative areas (Supplemental Figure 1). These results demonstrate that *Acvr1*$^{R206H/+}$ preosseous tissues are aberrantly stiffer and indicate that cells at sites of wound repair are actively constructing and experiencing a local microenvironment that has greater mechanical signaling properties than in control tissues.

Differences in ECM composition and collagen organization contribute to stiffer Acvr1$^{R206H/+}$ tissue

The biophysical properties of tissue can be altered by subtle differences in matrix composition and/or organization. During normal wound healing in muscle, fibro/adipogenic progenitors (FAPs) (Contreras *et al.*, 2016) secrete increased amounts of various collagen isoforms, a process that is correlated with increased tissue stiffening (Hinz *et al.*, 2012). Collagens are the major component of connective tissue ECM in mammals, forming a structural framework for cells and functioning as a storage system for morphogens and growth factors (Reddi, 2000). Collagen types I and III are the main collagens expressed by myofibroblasts during wound healing (Hinz, 2007; Hinz *et al.*, 2012; Watsky *et al.*, 2010; Klingberg *et al.*, 2013). We therefore investigated whether the elevated stiffness within *Acvr1*$^{R206H/+}$ lesions is accompanied by altered collagen content and organization within the fibroproliferative tissue.

To quantify changes in collagen production in further detail, we used mouse embryonic fibroblasts (MEFs) as an in vitro system. MEFs have properties of mesenchymal stem/progenitor cells including multipotent lineage potential (Lengner *et al.*, 2004; Garreta *et al.*, 2006; Saeed *et al.*, 2012; Culbert *et al.*, 2014). We previously demonstrated that *Acvr1*$^{R206H/+}$ MEFs can undergo adipogenesis, chondrogenesis, and osteogenesis and that the mutation induces accelerated chondrogenesis and endochondral ossification (Culbert *et al.*, 2014). *Acvr1*$^{R206H/+}$ MEFs also have increased BMP-pSmad1/5/8 pathway activation, a hallmark of FOP patient-derived cells that has been recapitulated and verified in multiple systems (Billings *et al.*, 2008; Shen *et al.*, 2009; Culbert *et al.*, 2014).

Total collagens produced by control and *Acvr1*$^{R206H/+}$ MEFs were visualized and quantified by picrosirius red staining of cell monolayers and showed increased collagen deposition in *Acvr1*$^{R206H/+}$ cells compared with control (Figure 2A). No differences in collagen type I mRNA levels were detected by quantitative reverse transcription-PCR (qRT-PCR) analysis; however, mutant cells expressed elevated collagen type II mRNA compared with controls (Figure 2B). Collagen type III expression appeared to be delayed in *Acvr1*$^{R206H/+}$ cells, with lower mRNA levels at earlier time points compared with controls.

To qualitatively assess collagens within control and *Acvr1*$^{R206H/+}$ injured muscle, collagens type I, type II, and type III were detected by immunostaining at the fibroproliferative stage (Figure 3A). Counterstaining with hematoxylin or 4′,6-diamidino-2-phenylindole (DAPI) was used to identify areas of intact muscle and damaged tissue. No qualitative differences were detected in collagen type I or

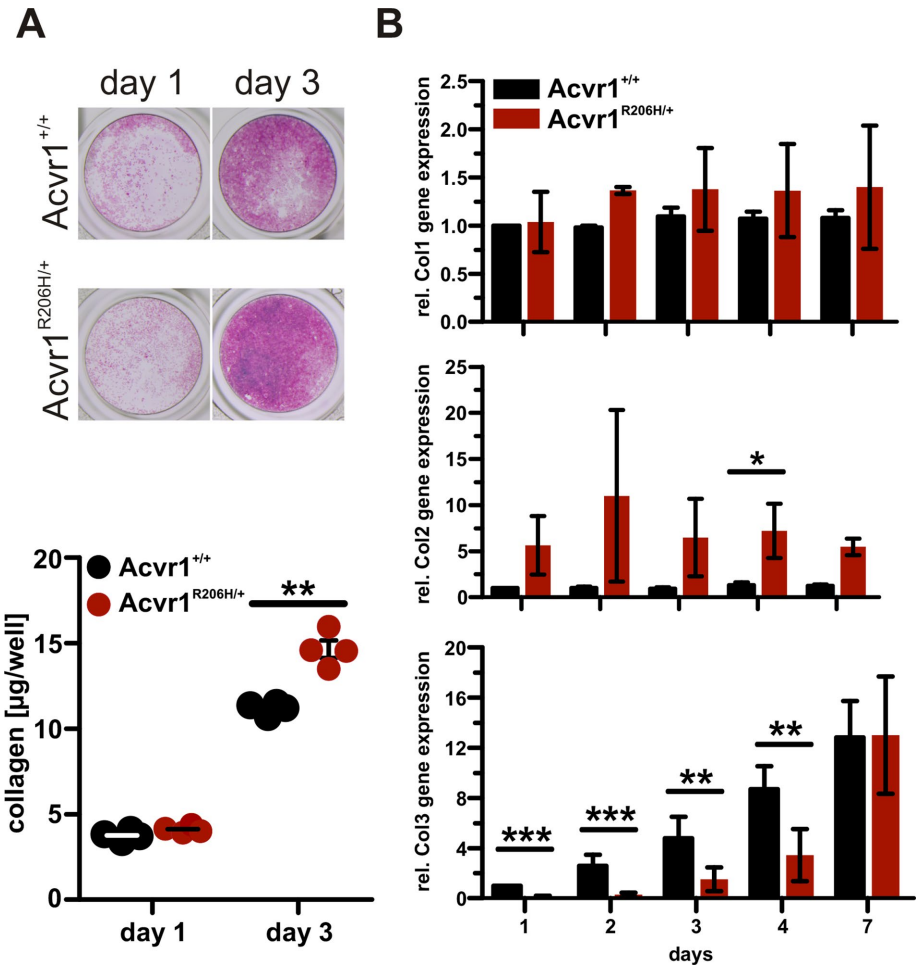

FIGURE 2: Altered collagen composition in Acvr1$^{R206H/+}$ cells. In vitro analyses of collagen deposition and gene expression were conducted in immortalized MEFs. (A) Sirius red/Fast green staining demonstrated increased collagen deposition in *Acvr1*$^{R206H/+}$ (FOP) cells compared with control (*Acvr1*$^{+/+}$). Fast green counterstain was used to normalize to total protein content after extraction. Graph represents mean ± SEM. Results from one representative experiment of three independent experiments are shown. (B) Collagen type I–III mRNA expression was quantified over time by RT-PCR. Data are relative to *Acvr1*$^{+/+}$ controls on day 1. *Acvr1*$^{R206H/+}$ cells showed increased collagen type II expression (day 1: $n = 5$; day 2: $n = 3$; day 3: $n = 4$; day 4: $n = 4$; day 7: $n = 3$). Graphs represent mean ± SEM. Significance was determined by two-tailed Student's *t* test; *$p < 0.05$; **$p < 0.01$; ***$p < 0.001$.

III deposition in either control or *Acvr1*$^{R206H/+}$ tissues at this stage of lesion progression. Collagen type II, a collagen associated with cartilage matrix, is not expressed by fibroblasts (Olsen *et al.*, 1989) and was not detected in control wounds; however, collagen type II was detected in fibroproliferative lesions of *Acvr1*$^{R206H/+}$ tissue, indicating improper collagen production resulting from the mutation following injury (Figure 3B).

This modified composition of extracellular matrix produced by *Acvr1*$^{R206H/+}$ cells and tissue prompted us to investigate in vivo structural differences more closely using second harmonic generation (SHG) imaging, a powerful approach for visualizing collagen organization in tissues (Chen *et al.*, 2012). The degree of collagen organization within the tissue following injury was determined by blinded scoring; higher scores indicate a more organized SHG-positive ECM and lower scores indicate a more disorganized arrangement. A higher degree of collagen organization suggesting increased density of fibrillar collagen was found in *Acvr1*$^{R206H/+}$ injured muscle at the fibroproliferative stage compared with control littermates (Figure 3, C and D), indicating advanced organization and maturation. Increased fibrillar density has been correlated with increased tissue stiffness and higher Young's modulus (Carroll *et al.*, 1989; Roeder *et al.*, 2002; Raub *et al.*, 2010), suggesting that changes in collagen organization contributes to the increased lesion stiffness in FOP. These findings suggest that altered ECM composition and organization in *Acvr1*$^{R206H/+}$ lesions contribute to redirecting cell fate decision of progenitor cells into chondrogenic and/or osteogenic lineages, although a more detailed mechanism of how this altered content and assembly culminates in increased tissue stiffening remains to be elucidated.

Mechanotransduction pathways are overactivated in Acvr1$^{R206H/+}$ cells

Cellular behavior of fibroblasts (e.g., differentiation, proliferation, ECM secretion) is strongly influenced by mechanical cues derived from the underlying substrata (Wells, 2008). Cells translate these physical forces from the microenvironment into biochemical signals that are intracellularly transmitted via multiple mechanoresponsive signaling pathways (Tzima, 2006). The Rho family of small GTPases activates one of the most studied mechanotransduction pathways and Rho signaling is a key regulator of the actin cytoskeleton. Rho cycles among inactive, GDP-bound and -active, and GTP-bound states, consequently regulating the activity of downstream effectors such as Rho kinase (ROCK), a critical regulator of cell contractility (Lessey *et al.*, 2012). Basal activation of BMP signaling pathways, even in the absence of ligand, also has been shown to regulate cell contractility in mesenchymal stem cells (Heo *et al.*, 2015, 2016).

To determine the influence of the *Acvr1*^{R206H} mutation on mechanosignaling, we first evaluated the basal activation level of the Rho/ROCK pathway in *Acvr1*$^{+/+}$ control and mutant *Acvr1*$^{R206H/+}$ MEFs. When cultured on tissue culture plastic, which presents a very stiff substrate (Achterberg *et al.*, 2014), Rho activation was more robustly increased in *Acvr1*$^{R206H/+}$ cells compared with controls (Figure 4A). RhoA, a small GTPase, regulates its kinase effector ROCK to influence actin filament stability and cytoskeletal organization and contractility by controlling the activity of its downstream targets cofilin and myosin light chain 2 (MLC2) (Riento and Ridley, 2003; Lessey *et al.*, 2012; Smith *et al.*, 2018). Cofilin affects cytoskeletal organization and dynamics by acting as a severing and disassembling protein of actin filaments; Rho/ROCK-mediated signaling phosphorylates and inactivates cofilin, thereby stabilizing actin-myosin filaments (DesMarais *et al.*, 2005). Rho signaling through ROCK can induce contractility of the actomyosin cytoskeleton either by directly activating MLC2 through phosphorylation or indirectly by inhibiting its antagonist myosin-light-chain phosphatase (Riento and Ridley, 2003). Consistent with increased Rho activation, *Acvr1*$^{R206H/+}$ cells showed elevated levels of phospho-Cofilin (Figure 4B) and

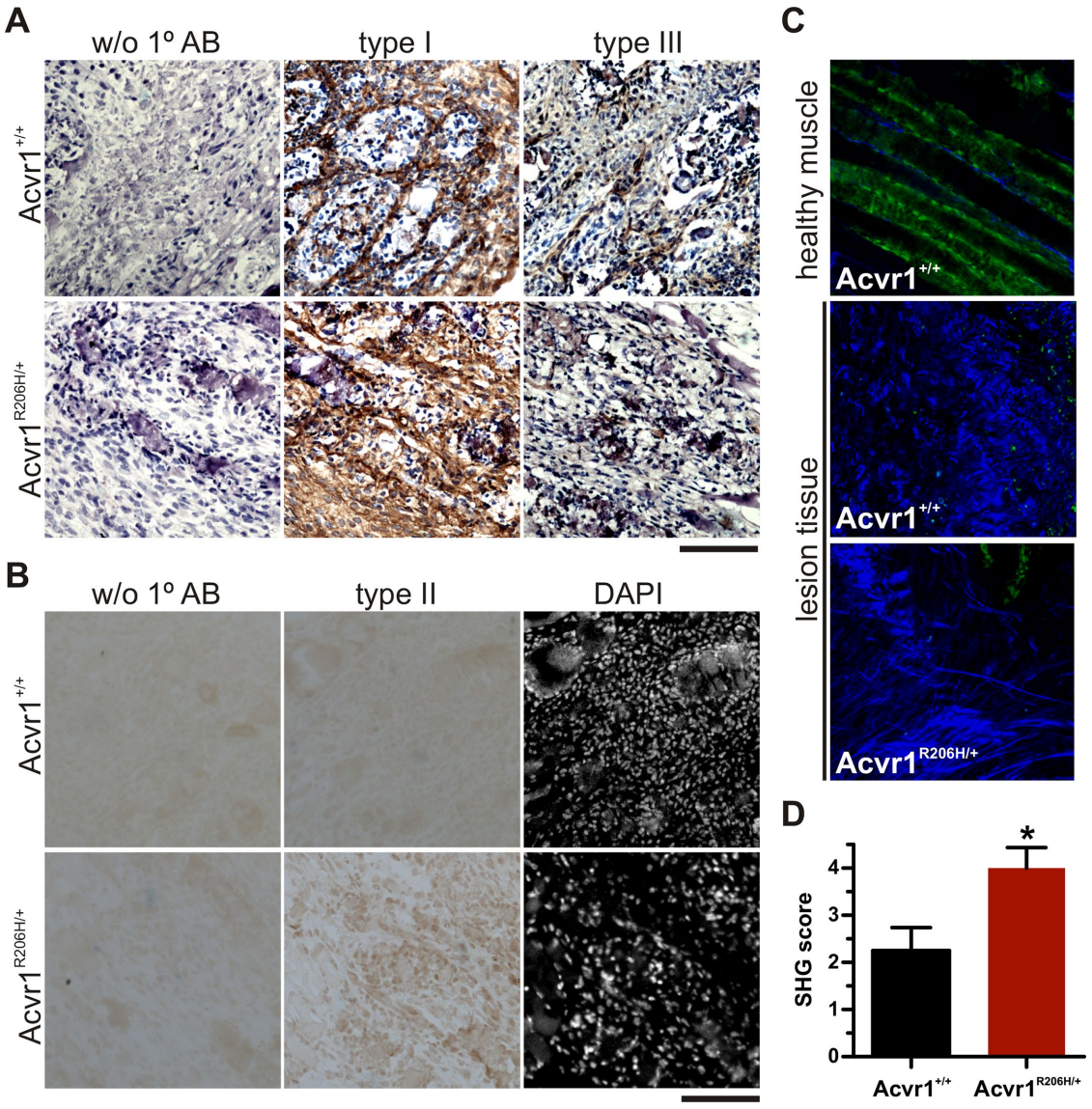

FIGURE 3: Altered ECM composition and organization in lesions from *Acvr1*$^{R206H/+}$ mice. (A, B) Tissues from cardiotoxin injected quadriceps 5 d post–injection of FOP mice or littermate controls were counterstained with (A) hematoxylin after collagen types I and III immunostaining or (B) DAPI after collagen type II detection. *Acvr1*$^{R206H/+}$ lesions did not show qualitative differences in collagen type I or III deposition during the fibroproliferative stage, but collagen type II was more highly detected (brown stain). Scale bar represents 100 μm. (C) Representative images from SHG (blue signal) were used to quantify differences in collagen organization (D) between FOP ($n = 7$) and control littermates ($n = 8$) at the fibroproliferative stage. Significance was determined by two-tailed Student's *t* test; *$p = 0.02$.

phospho-MLC2 (Figure 4C) compared with controls, confirming overactivation of this mechanotransduction pathway in mutant cells cultured on rigid substrates.

Nuclear stiffness also has been shown to scale with substrate rigidity (Swift *et al.*, 2013) and can be measured by AFM indentation of the cell in the perinuclear region (Figure 5A), with this measurement of nuclear stiffness being a strong indicator of the overall contractile state of the cell (Swift *et al.*, 2013). Consistent with changes in the bulk contractile state of the cells, *Acvr1*$^{R206H/+}$ MEF cells on rigid substrates showed increased nuclear stiffness compared with *Acvr1*$^{+/+}$ controls (Figure 5B and Supplemental Material 2). Nuclear height also decreases as a function of cytoskeletal contraction on two-dimensional culture substrates (Versaevel *et al.*, 2012) due to the increased contractility of the perinuclear actin cytoskeleton that compacts the nucleus. We found significant flattening of *Acvr1*$^{R206H/+}$ nuclei in comparison to control cells (Figure 5C, left). This nuclear flattening was rescued by reducing cellular contractility through treatment with the ROCK inhibitor Y-27632 (Y27) (Figure 5C, right), supporting that an inherently higher baseline contractility causes changes in the nuclear height/morphology of *Acvr1*$^{R206H/+}$ cells, providing additional evidence of increased mechanical signaling activity in mutant cells. Taken together, these data indicate that the Rho/ROCK mechanotransduction pathway is overactivated in *Acvr1*$^{R206H/+}$ cells, supporting an altered biomechanical response and misinterpretation of the substrate as a contributing mechanism to FOP pathology.

Acvr1$^{R206H/+}$ cells misinterpret substrate rigidity

The above studies, conducted on tissue culture plastic, support increased activation of mechanotransduction pathways by *Acvr1*$^{R206H/+}$ cells. Such stiff substrates inherently increase mechanosignaling

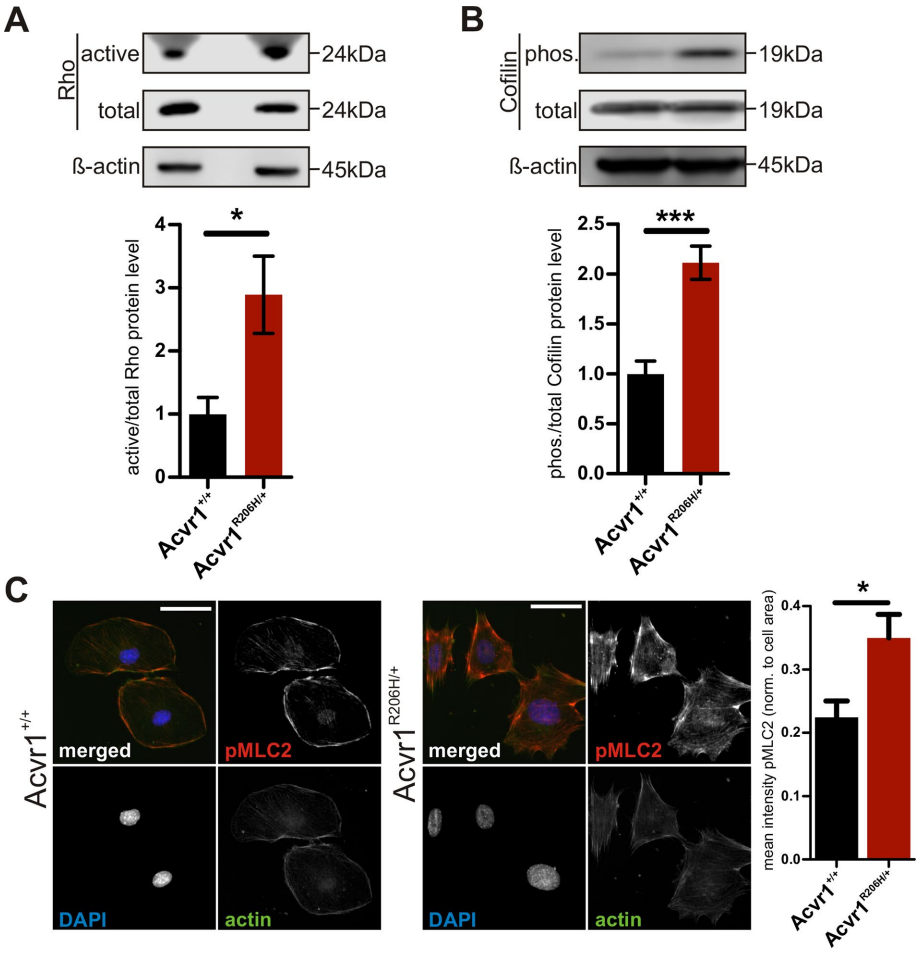

FIGURE 4: Increased signaling through mechanosensing pathways in *Acvr1*$^{R206H/+}$ cells. (A) Increased activation of mechanotransduction in *Acvr1*$^{R206H/+}$ (FOP) cells was determined by immunoblot for Rho after pull down of the active form ($n = 6$). Active Rho protein was normalized to total Rho. (B, C) Detection of RhoA downstream targets cofilin by immunoblot for pCofilin ($n = 5$) and MLC2 by immunostaining for pMLC2 showed increased levels in *Acvr1*$^{R206H/+}$ cells. pCofilin was normalized to total cofilin protein. Quantification of mean intensity of pMLC2 staining from three independent experiments normalized to cell area (*Acvr1*$^{+/+}$ $n = 61$ *Acvr1*$^{R206H/+}$ $n = 91$). Scale bar represents 50 µm. Graphs represent mean ± SEM. Significance was determined by two-tailed Student's *t* test; *$p < 0.05$; ***$p < 0.001$.

(Wipff *et al.*, 2007; Hinz, 2010; Tee *et al.*, 2011; Thomas *et al.*, 2014; Young *et al.*, 2014) and may mask differences by activating pathways that are normally quiescent on a physiologic (softer) stiffness. To further test altered stiffness sensing by *Acvr1*$^{R206H/+}$ cells, we used a polyacrylamide (PA)-hydrogel culture system to produce physiologically-stiff substrates with rigidities that mimic the mechanical properties of various tissues (Engler *et al.*, 2006; Aratyn-Schaus *et al.*, 2010; Ivanovska *et al.*, 2017). Thin layers of PA-hydrogels ($h =$ 100 µm) were polymerized onto glass slides followed by coating with fibronectin to facilitate cell attachment. Hydrogel stiffness was controlled by acrylamide content, and the resulting stiffness verified by AFM force spectroscopy. Since cell–cell contacts can override cell-ECM-induced mechanosignaling (Maruthamuthu *et al.*, 2011), fibroblasts were seeded at low cell densities.

Response to the underlying substrate was quantified by measuring cell area and cell shape (aspect ratio) following cytoskeleton staining with phalloidin. As expected, both morphological parameters scale with substrate rigidity in *Acvr1*$^{+/+}$ control cells, as determined by increased cell spreading (greater cell area and less circular shape) with increasing substrate stiffness (Figure 6, A and B). In contrast, *Acvr1*$^{R206H/+}$ cells showed reduced responsiveness to substrate stiffness as evidenced by the consistently higher cell size and morphology of the mutant cells across increasing rigidity. Overall, *Acvr1*$^{R206H/+}$ cells exhibited significantly greater cell areas and spreading compared with control cells; this was most pronounced for *Acvr1*$^{R206H/+}$ cells on softer matrices (5 kPa) which exhibited spread areas similarly to control cells on much stiffer substrates (15 kPa). These findings indicate that, in addition to creating a stiffer tissue microenvironment in FOP lesions, *Acvr1*$^{R206H/+}$ cells may also misinterpret and/or be less sensitive to the mechanical cues provided by their tissue environment during injury, inducing progenitor populations to follow abnormal lineage commitment pathways.

To investigate whether altered mechanosensing is associated with an osteogenic response in *Acvr1*$^{R206H/+}$ cells on softer substrates, we examined a key pro-osteoblast factor runt related transcription factor 2 (RUNX2; alias: CBFA1) that has been shown to be essential during early commitment of mesenchymal stem cells to the osteogenic lineage (Ducy *et al.*, 1997; Komori *et al.*, 1997; Otto *et al.*, 1997; Kobayashi *et al.*, 2000). Nuclear localization of RUNX2 is critical for its ability to act as a transcription factor to induce the expression of genes required for osteogenesis such as alkaline phosphatase, osteocalcin, and osterix (Komori *et al.*, 1997; Xiao *et al.*, 2000; Almalki and Agrawal, 2016). Previous work has shown that matrix stiffness regulates the nuclear localization of this factor in stem cells (Yang *et al.*, 2014; Cosgrove *et al.*, 2016), with stiffer substrates promoting more nuclear localization.

Acvr1$^{+/+}$ control and mutant *Acvr1*$^{R206H/+}$ MEFs were cultured on PA-hydrogels of various stiffnesses for 18 h, immunostained for RUNX2 protein localization (Figure 7A), and quantified for nuclear:cytoplasmic localization ratios of RUNX2 (Figure 7B). We found that on all substrate stiffnesses tested, RUNX2 nuclear localization was higher in *Acvr1*$^{R206H/+}$ compared with *Acvr1*$^{+/+}$ control cells (Figure 7B). Differences were most pronounced on 10 kPa, a stiffness comparable to normal muscle tissue (Engler *et al.*, 2006). Since heterotopic bone forms within skeletal muscle tissue in patients with FOP, the difference in RUNX2 protein localization at 10 kPa stiffness may be functionally relevant. Taken together, these data strongly support that *Acvr1*$^{R206H/+}$ cells misinterpret their biophysical microenvironment, which leads to important changes in key factors that direct cellular differentiation and extracellular matrix production.

DISCUSSION

Heterotopic ossification in the rare genetic disorder FOP, as well as in more common nonhereditary HO, forms through a progressive series of tissue/cellular events that culminate in bone formation

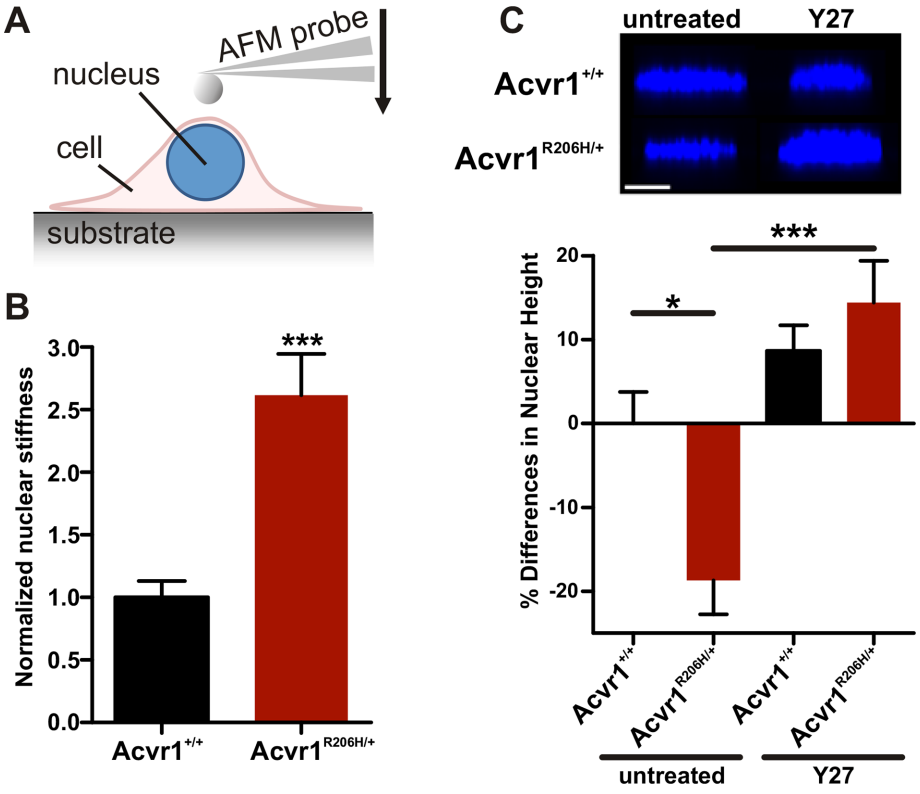

FIGURE 5: Increased nuclear stiffness and altered nuclear height in *Acvr1*$^{R206H/+}$ cells. (A) Schematic of nuclear stiffness measurement by AFM. (B) Quantification of nuclear stiffness determined by AFM indicates higher stiffness in *Acvr1*$^{R206H/+}$ cells compared with controls (*Acvr1*$^{+/+}$) (both $n = 20$). (C) Nuclear height in MEFs was determined by confocal microscopy, before (untreated) and after treatment with 10 μM Y-27632 (Y27), a ROCK inhibitor, for 1 h ($n =$ 15–20 cells/group). Untreated *Acvr1*$^{R206H/+}$ cells show nuclear flattening (relative to control cells; i.e., negative value: *Acvr1*$^{+/+}$: $n = 15$; *Acvr1*$^{R206H/+}$: $n = 20$). The flattened morphology was rescued by reducing cellular contractility with the ROCK inhibitor Y-27632 (*Acvr1*$^{+/+}$: $n = 18$ *Acvr1*$^{R206H/+}$: $n = 19$). Scale bar represents 10 μm. Graphs represent mean ± SEM. Statistical significance was determined by two-tailed Student's *t* test, ***$p < 0.001$ (in B); or one-way ANOVA, *$p < 0.05$, ***$p < 0.001$; Bonferroni's post hoc (in C).

within skeletal muscle and other connective tissues in response to tissue injury (Kaplan *et al.*, 1993; Shore and Kaplan, 2010; Convente *et al.*, 2018). During normal response to injury, resident fibroblasts at the wound site become activated myofibroblasts and this fibroproliferative stage is followed by the recruitment of muscle stem cells to regenerate muscle tissue (Charge and Rudnicki, 2004). In the presence of the *ACVR1*^{R206H} mutation, injury triggers the removal of damaged tissue and stimulates fibroproliferation, but cartilage and bone tissue subsequently form at the expense of muscle regeneration (Shore and Kaplan, 2010; Convente *et al.*, 2018). The cellular response during this fibroproliferative tissue stage therefore may provide key insight into the cellular mechanisms that regulate heterotopic ossification. Cell fate is regulated by multiple factors including extracellular ligands, such as BMPs, and physical/mechanical signals from the cell microenvironment, such as the stiffness of the surrounding tissue (Engler *et al.*, 2006; Wang *et al.*, 2014; Dingal *et al.*, 2015; Salazar *et al.*, 2016; Discher *et al.*, 2017).

All cells sense physical cues, including the stiffness of their environment. When these biophysical cues change, cell phenotype has the potential to be altered as a result (Guilak *et al.*, 2009; Irianto *et al.*, 2016). In this study, we investigated whether the *Acvr1*$^{R206H/+}$ mutation additionally influences the physical properties of tissues and/or the cell response to the tissue microenvironment. Such changes could provide the permissive conditions that support subsequent progression of aberrant cell differentiation to heterotopic bone and could provide novel targets for therapeutic intervention.

Using an in vivo model (*Acvr1*$^{R206H/+}$ knock-in mouse) of injury-induced heterotopic ossification and AFM to directly measure the physical stiffness of the tissue, we determined that the FOP mutation results in the aberrant production of a stiff, fibrotic-like environment at an early stage of repair and prior to the production of ectopic bone by mutant tissue. Our data suggest that *Acvr1*$^{R206H/+}$ cells involved in tissue repair establish a microenvironment that favors heterotopic bone formation.

ECM organization and composition, notably of collagens, are key determinants of tissue stiffness, and we determined that the fibroproliferative tissue in FOP lesions was organized to a greater extent than tissue in control lesions. Type I and type III collagens were detected at similar levels in *Acvr1*$^{R206H/+}$ and *Acvr1*$^{+/+}$ control lesions. However, type II collagen, which is usually restricted to specific tissues such as cartilage and is an established secondary target gene of the BMP signaling pathway (Olsen *et al.*, 1989; Bell *et al.*, 1997; Ng *et al.*, 1997) was increased only in mutant repair tissue, consistent with overactivation of the BMP signaling pathway by the *Acvr1*$^{R206H/+}$ mutation. In cartilage, the type II collagen network traps negatively charged proteoglycan aggregates that imbibe water into the tissue generating compressive stiffness (Burg *et al.*, 1996; Majd *et al.*, 2014) and therefore type II collagen in *Acvr1*$^{R206H/+}$ lesions may also cause increased stiffening in part by increasing hydration/swelling of lesion tissue and/or improper accumulation of proteoglycans.

Cells interpret the biophysical properties of their surroundings via cell surface mechanoreceptors that are coupled to the contractile cytoskeleton and signal through several direct and indirect signaling pathways that direct cell fate through modification of chromatin organization and gene expression (Arnsdorf *et al.*, 2009; Swift *et al.*, 2013; Smith *et al.*, 2017, 2018). We determined that the Rho/ROCK mechanosignaling pathway, which mediates signals from the extracellular matrix, integrins, and focal adhesions that affect cellular morphology, migration, contractility, and adhesion to surface substrates (Lessey *et al.*, 2012), is overactivated in cells with the *Acvr1*$^{R206H/+}$ mutation and that mutant cells additionally show increased nuclear and cellular stiffness, supporting that they do not correctly sense and interpret physical/mechanical cues from their tissue microenvironment. RhoA also facilitates phosphorylation of Smad1/5/8 (Derynck and Zhang, 2003; Du *et al.*, 2011; Wang *et al.*, 2012; Kopf *et al.*, 2014), creating a further connection between RhoA activation and BMP signaling, two critical pathways that impact cell fate. Given the association between RhoA and osteogenic commitment (Arnsdorf *et al.*, 2009), our data suggest that RhoA and BMP pathways might act synergistically to contribute to

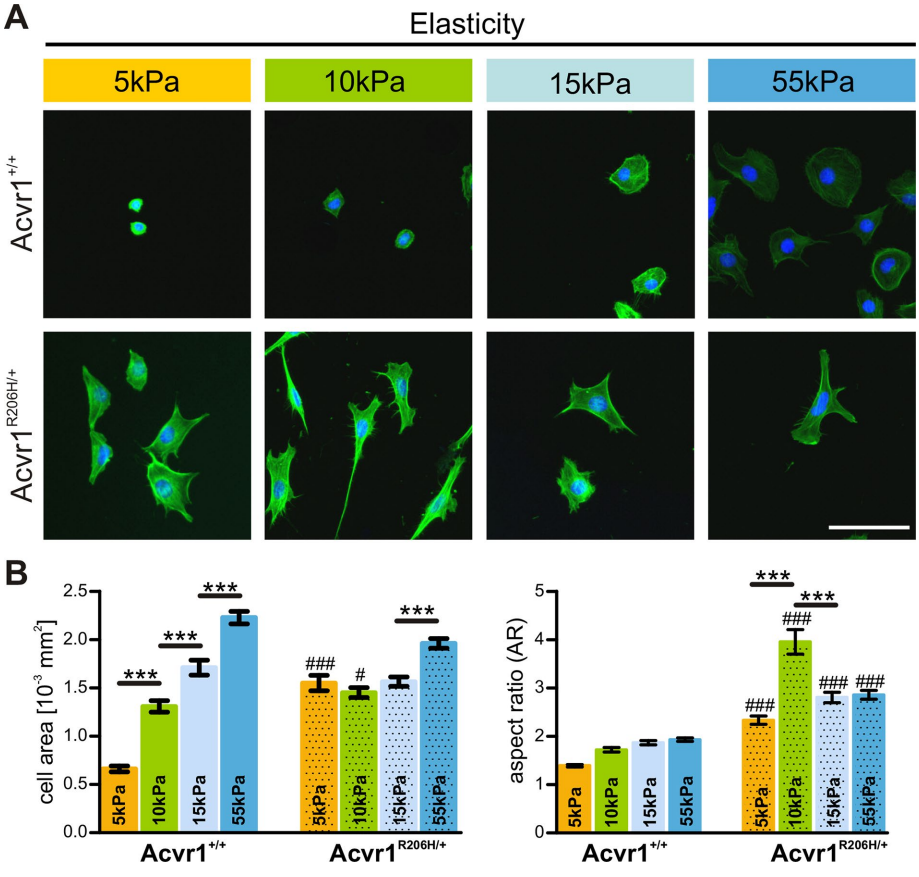

FIGURE 6: *Acvr1*$^{R206H/+}$ cells misinterpret substrate elasticity. (A) Immortalized control and *Acvr1*$^{R206H/+}$ (FOP) cells on gels of various rigidities (5, 10, 15, and 55 kPa) were stained with phalloidin and DAPI. (B) Cell area and aspect ratio (AR) were measured as a function of matrix elasticity. Graphs represent mean ± SEM of >350 cells from four independent experiments. Significance was determined by two-way ANOVA (comparison between genotypes; Tukey–Kramer adjustment; $^{\#}p < 0.05$, $^{\#\#\#}p < 0.001$, NS = not significant) or one-way ANOVA (comparison between substrate stiffness; $^{***}p < 0.001$; Bonferroni's post hoc). Scale bar represents 100 µm.

chondrogenic and osteogenic differentiation and endochondral ossification in FOP.

Acvr1$^{R206H/+}$ cells mesenchymal progenitor cells incorrectly sensed and interpreted substrate stiffness, responding with a considerably spread morphology on even very soft substrates. Strikingly, this response to the physical/mechanical environment was accompanied by increased nuclear localization of RUNX2, a chondro/osteogenic transcription factor (Komori *et al.*, 1997; Xiao *et al.*, 2000; Wang *et al.*, 2005; Chen *et al.*, 2014; Almalki and Agrawal, 2016). BMPs induce expression of RUNX2 (Hay *et al.*, 2001; Matsubara *et al.*, 2008; Sun *et al.*, 2015) and RUNX2 nuclear localization is positively affected by increased mechanical force (Zhang *et al.*, 2012; Yang *et al.*, 2014; Jazayeri *et al.*, 2015; Cosgrove *et al.*, 2016), supporting that increased BMP-pSmad1/5/8 signaling by the mutant *Acvr1*^{R206H} receptor together with misinterpretation of microenvironment contribute to aberrant chondro/osteogenic differentiation by *Acvr1*$^{R206H/+}$ cells.

This study identifies for the first time that the FOP mutation alters cell mechanical state and mechanobiology, as well as the material properties of the wound microenvironment. We found that FOP cells are less sensitive to changing physical/mechanical features than control cells and that FOP tissue healing causes wounded muscle tissue to repair in a manner that is stiffer and more organized than normally occurs during skeletal muscle injury. These data support that the physical tissue microenvironment in which heterotopic ossification forms is both altered by cells with the *ACVR1*^{R206H} mutation and is differentially perceived by cells with the *ACVR1*^{R206H} mutation. We additionally propose that initial small-scale changes in the ECM (such as collagen type II production) act to prime formation of a stiffer tissue microenvironment. That is, BMP pathway signaling by the Acvr1^{R206H} mutation alters the repair trajectory of injured tissue, with cells interpreting softer matrices as stiffer. As tissue resident mesenchymal cells, such as the FAPs that have recently been identified as a major source of HO forming cells in a mouse model of FOP (Lees-Shepard *et al.*, 2018), begin to respond to the stiffer environment in the context of enhanced BMP pathway signaling, a reinforcing feedback loop results. This furthers ECM production and tissue stiffening (a situation that alone is pathologic, such as in fibrosis), but in the context of increased BMP signaling and altered biomechanical sensing, the cells are directed to differentiate to form heterotopic bone.

A novel treatment strategy to prevent HO formation in FOP patients, and potentially more common, nonhereditary forms of HO, may reside in the regulation of mechanotransduction pathways during tissue repair (e.g., Fasudil [selective ROCK inhibitor], Cethrin [Rho inhibitor]) (Shimizu *et al.*, 2001; Liao *et al.*, 2007; Fehlings *et al.*, 2011; Bei *et al.*, 2013; Zhou *et al.*, 2013). Our findings of biomechanical cues are important to consider in light of a recent therapeutic approach that has been successfully used in animal models to ameliorate fibrosis and also suggested to treat solid tumors that show increased stiffness and mechanical properties (Jain *et al.*, 2014; Kai *et al.*, 2016). Taken together, our data reveal the importance of mechanobiological signaling in FOP cells and provide the first direct experimental evidence that FOP progression may be influenced by the tissue microenvironment. Further studies will investigate the dependence on an altered physical environment to support heterotopic ossification, altered mechanosensing by progenitor cells, and the effects of inhibitors of biomechanical effectors on chondro/osteogenic differentiation in *Acvr1*$^{R206H/+}$ cells.

MATERIALS AND METHODS

Mouse strain and animal care and use

Cells (MEFs) for in vitro experiments were obtained from *Acvr1*$^{R206H/+}$ knock-in mice described in Chakkalakal *et al.* (2012).

Tissues for in vivo studies were obtained from *Acvr1*$^{[R206H]FlEx}$ conditional-on knock-in mice (Hatsell *et al.*, 2015; Chakkalakal *et al.*, 2016) that were bred to include R26-rtTA and tetO-Cre as described (Chakkalakal *et al.*, 2016; Convente *et al.*, 2018). Here we refer to these mice as *Acvr1*$^{R206H/+}$. Acvr1$^{+/+}$ controls were littermates that did not contain an Acvr1^{R206H} allele (as verified via PCR genotyping). To induce recombination and global expression of the mutant allele,

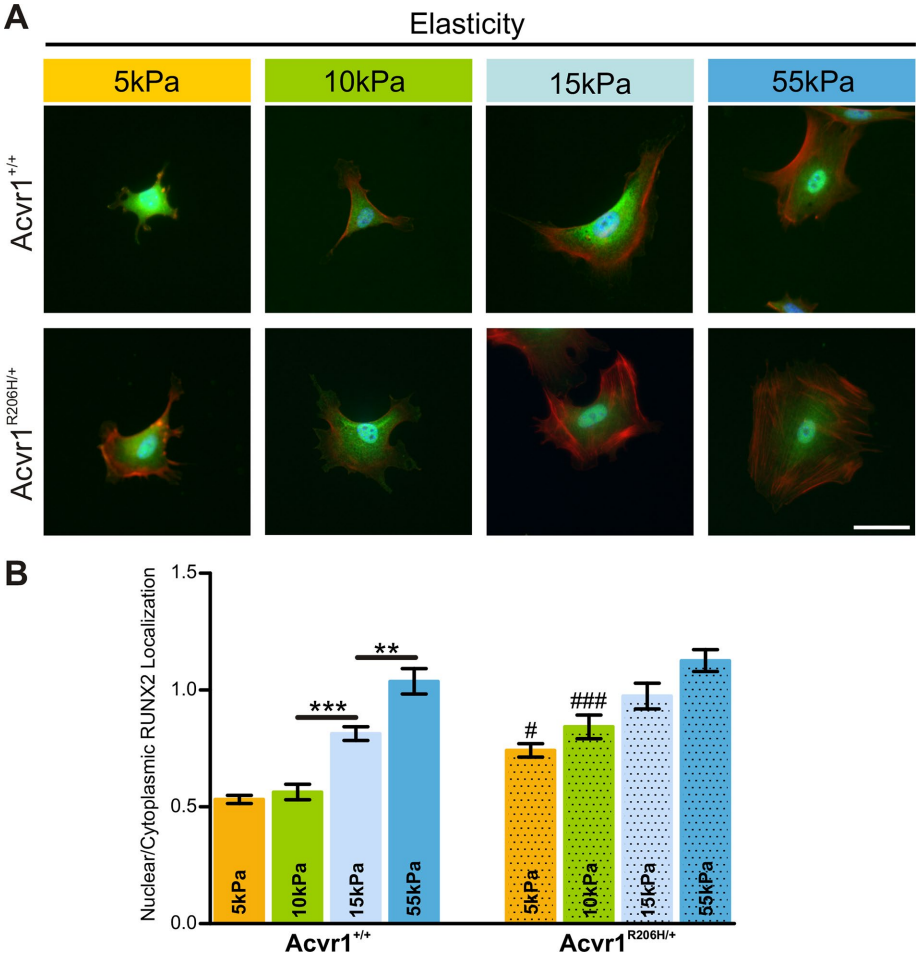

FIGURE 7: RUNX2 nuclear localization is increased in FOP cells. (A) Immortalized *Acvr1*$^{+/+}$ control and *Acvr1*$^{R206H/+}$ cells on substrates of various rigidities (5, 10, 15, and 55 kPa) were detected for RUNX2 (green), phalloidin (red), and DAPI (blue). Nuclear localization of RUNX2 protein indicates activation of osteogenic cell fate programming. Scale bar represents 50 μm. (B) Relative nuclear localization of RUNX2 was quantified by the ratio of nuclear/cytoplasmic staining. Intensity shows that *Acvr1*$^{R206H/+}$ cells have more nuclear RUNX2 on softer substrates compared with *Acvr1*$^{+/+}$ control cells. Nuclear localization on stiffer substrates does not differ significantly between the genotypes, as expected. Graph represents mean ± SEM. Assay was repeated in three independent experiments ($n = 50$ cells per substrate stiffness per experiment). Statistical significance relative to *Acvr1*$^{+/+}$ controls at a given substrate stiffness (**$p < 0.01$, ***$p < 0.001$) or comparison between genotypes ($^{\#}p < 0.05$, $^{\#\#\#}p < 0.001$) were determined by one-way ANOVA (Bonferroni's post hoc).

4-wk-old mice were provided a doxycycline diet (either 200 or 625 mg/kg) for at least three consecutive days. Cre-mediated recombination was verified by PCR. Littermate Acvr1$^{+/+}$ controls were also treated with doxycycline. Mice were not assigned to treatment groups by gender in our experiments.

Induction of lesions in muscle tissue

Mouse quadriceps muscles were injected with 100 μl CTX solution (10 μM in phosphate-buffered saline [PBS]; Calbiochem). Muscle injury by CTX injection is a standard experimental approach in muscle regeneration studies (Couteaux *et al.*, 1988; Charge and Rudnicki, 2004; Vignaud *et al.*, 2005; Czerwinska *et al.*, 2012). PBS injection in *Acvr1*$^{R206H/+}$ and *Acvr1*$^{+/+}$ littermates served as controls. This approach for injury induction of HO has been well characterized (Chakkalakal *et al.*, 2016; Convente *et al.*, 2018), with heterotopic bone forming at 10–14 d and robust fibroproliferation at 4–5 d. Animals were killed at the fibroproliferative stage to isolate lesion tissue and surrounding skeletal muscle. Tissues were embedded in optimal cutting temperature media (OCT; CryoPrep; American MasterTech Scientific) and serially sectioned at 20-μm thickness for AFM analysis or 10 μm for histology and immunohistochemistry.

Histology and collagen immunohistochemistry

Tissues were fixed in 4% paraformaldehyde (PFA) in PBS (Fisher Scientific), sectioned to 10 μm, and stained with Harris modified hematoxylin and eosin Y (H&E) or used for immunohistochemistry.

For collagen detection, endogenous peroxidases were quenched by incubation with 3% hydrogen peroxidase solution. Sections were blocked (Background Buster; American MasterTech) and incubated overnight at 4°C with primary antibody against collagen type I and II (Abcam; catalogue ab34710 and ab21291, respectively), collagen type III (Thermo Scientific; catalogue PA5-27828), or IgG control (Cell Signaling Technology; catalogue 3900). After incubation with HRP-linked secondary anti-rabbit antibody (Cell Signaling Technology; catalogue 7074), signal was visualized by using 3,3′-diaminobenzidine (DAB) substrate (SuperPicTure Polymer; Invitrogen). Sections were counterstained by short incubation with hematoxylin (Vector Laboratories) or by DAPI using Fluoromount-G (SouthernBiotech). Imaging was carried out using an Eclipse 90i microscope (Nikon).

Analysis of tissue and cellular stiffness using atomic force microscopy

Tissue and nuclear stiffness were measured via nanoindentation using an atomic force microscope equipped for simultaneous optical imaging (Agilent ILM 6000 mounted on a Nikon inverted microscope) (Roduit *et al.*, 2009; Thomas *et al.*, 2013; Heo *et al.*, 2016). For tissue analysis, unfixed 20-μm cryosections were hydrated and probed using cantilevers with 1-μm spherical tips and a nominal spring constant of a 0.6 N/m (Novascan). For each location measured, four force curves were collected over a 15 μm × 15 μm region that was visually identified as healthy muscle, degrading muscle, or fibroproliferative lesion tissue. For nuclear measurements, the AFM stage was maintained at 37°C. Cells were probed using silicon nitride cantilevers with 1 μm spherical tips and a nominal spring constant of 0.06 N/m (Novascan); force maps of up to 16 force curves were collected above the cell nucleus. For all measurements, actual cantilever spring constants were determined via the thermal fluctuation method. For both tissue and cell measurements, the first 300 nm of indentation was fitted using a Hertzian contact model to estimate stiffness (elastic modulus). After applying the Grubbs' test for outliers, estimated moduli were averaged over each tissue location or cell and considered as one data point.

Second-harmonic generation

To visualize collagen organization, SHG imaging (Han *et al.*, 2016) of unstained, unfixed 20-µm cryosections was performed using an excitation wavelength of 800 nm (Zeiss LSM 510 with tunable Ti-Sapphire laser). Signal collected between 390 and 465 nm was considered to be SHG specific, while signal collected between 500 and 550 nm was considered to be nonspecific tissue autofluorescence and used as a control. To semiquantitatively assess SHG images (n = 7–8 per genotype), four scorers blinded to genotype scored images on a categorical scale from highly organized (score = 5) to completely disorganized (score = 1). For each image, scores were averaged and considered as a single data point that is shown in the Figure 3D boxplot; genotype score was compared using a Student's *t* test.

Preparation of polyacrylamide hydrogels

Rigidity of native tissues was mimicked using an adjustable PA hydrogel system. PA hydrogels were prepared as described (Aratyn-Schaus *et al.*, 2010). Elastic moduli of the gels were verified through AFM force spectroscopy. Fibronectin (20 mg/ml) coating of gel surfaces was accomplished after treatment with 2 mg/ml sulfo-SANPAH (No. 22589; Pierce Protein Biology/Life Technologies, Rockford, IL) as described previously (Aratyn-Schaus *et al.*, 2010).

Cell culture, mouse embryonic fibroblasts, and in vitro assays

Knock-in *Acvr1*$^{R206H/+}$ MEFs were isolated at embryonic day 13.5 (E13.5) as previously described (Culbert *et al.*, 2014) from mice described in Chakkalakal *et al.* (2012) and from wild-type *Acvr1*$^{+/+}$ mice. Cells were immortalized (Capital Biosciences, Rockville, MD) by transducing cells with recombinant lentivirus expressing SV40 large T antigen. Expression of SV40 T antigen was confirmed via quantitative reverse transcription PCR (qRT-PCR). Genotypes of immortalized cell lines (iMEFs) and presence of the R206H mutation were confirmed by DNA sequencing. Cells were cultured in high glucose DMEM (Life Technologies) containing 10% fetal calf serum (FCS; Invitrogen). Testing for mycoplasma contamination was done after immortalization and repeated at the beginning of cultivation.

For nuclear height measurement, iMEFs were cultured in a standard growth medium (HG-DMEM, 10% FCS, 1% penicillin/streptomycin/fungiezone [PSF]), before treatment with ROCK inhibitor Y-27632 (Calbiochem; catalogue 688000) at 10 µM for 1 h. Following treatment, cells were fixed with 4% PFA, permeabilized with TX-100, and stained with DAPI. Nuclei (15–20 cells per condition) were imaged using a 100× 1.45 NA objective with a 1.7× zoom (0.07 µm/px) and a pinhole of 0.15 µm (0.5 AU) on a Nikon A1R Confocal Microscope. Measurements of nuclear height were determined from maximum projection XZ sections using the ImageJ software suite.

For mechanosensing assays, subconfluent iMEFs were seeded onto freshly prepared PA-hydrogels (described above) at a concentration of 5×10^3 cells/cm^2. After 16 h, cells on hydrogels were fixed in 4% paraformaldehyde/PBS (Affymetrix), followed by incubation with Alexa Fluor 488 Phalloidin (Invitrogen; catalogue A12379) to visualize the actin cytoskeleton and DAPI for nucleus staining. Cell contractility was visualized with primary pMLC2 antibody (Cell Signaling Technologies; catalogue 3674) followed by detection with AlexaFluor 594 anti-rabbit antibody (Invitrogen; catalogue A22107MP). RUNX2 protein localization was visualized with primary RUNX2 antibody (Cell Signaling; catalogue 12556; 1:800), followed by detection with Alexa Fluor 488 anti-rabbit antibody (Invitrogen; catalogue A12379; 1:1000); Alexa Fluor 546 phallodin (Invitrogen; catalogue A22283; 1:1000) was used to label F-actin simultaneously. Slides were mounted with DAPI Fluoromount-G (SouthernBiotech). Imaging used an Eclipse 90i microscope (Nikon) at consistent exposure times. Cell morphology was analyzed in ImageJ.

RUNX2 localization data were obtained through imaging immunostained cells (Eclipse 90i microscope; Nikon). Nuclear images were utilized to delineate the nuclear area from the cytoplasmic region, and the average fluorescent intensity over each region was calculated using ImageJ.

For collagen staining, cells were seeded in quadruplicates into a 96-well format at 2×10^3 cells/well. Total tissue collagen was detected (Sirius Red/Fast Green collagen staining kit; Chondrex; catalogue 9046). After imaging, incorporated dyes were extracted and measured at OD_{540} (for collagen) and OD_{605} (for noncollagen protein). Collagen content was calculated as µg/well following manufacturer's instructions.

Western blotting

Cells were lysed in buffer (RIPA; Sigma-Aldrich) supplemented with Halt Protease and Halt Phosphatase Inhibitor Cocktails (Pierce), cleared by centrifugation and quantified using BCA Protein Kit (Thermo Scientific). Proteins were electrophoresed through 10% Tris–glycine gels (Invitrogen) and transferred onto a nitrocellulose membrane (Invitrogen). Membranes were blocked in 5% milk in Tris-buffered saline (TBS) and incubated overnight at 4°C with primary antibody for cofilin, phospho-Cofilin, and β-actin (all Cell Signaling Technology; catalogue 5175, 3313, and 4967, respectively) followed by detection using a HRP-conjugated secondary antibody (Cell Signaling Technology; catalogue 7074). Membranes were incubated with HRP substrate (LI-COR) and chemiluminescence was detected and quantified with a C-DiGit Blot Scanner (LI-COR). Phospho- and total cofilin values were first normalized to β-actin to correct for variation in protein loading, followed by normalization of phospho- to total cofilin and, finally, to *Acvr1*$^{+/+}$ control cells.

Rho activity assay

Cells were cultured to confluence in 15-cm plates to obtain sufficient protein amounts for active Rho pull down. Cell lysis and pull down of active Rho used 550 µg of total protein following manufacturer's instructions (Active Rho Pull-Down and Detection Kit; Thermo Scientific; catalogue 16116). Proteins were electrophoresed through 10% Tris–glycine gels (Invitrogen), transferred onto nitrocellulose membranes (Invitrogen) and detected with anti-Rho antibody. Additional blots for total Rho and β-actin were run for all samples as loading controls.

RNA isolation and real-time RT-PCR analysis

RNA was isolated from MEF monolayers using TRIzol (Invitrogen). Genomic DNA was eliminated from RNA samples by digestion with RNase-free DNase (Promega). RNA concentration was determined by NanoDrop and equivalent amounts for each sample were used for cDNA synthesis using High Capacity RNA-to-cDNA reagents (Applied Biosystems). Quantitative PCR analysis was performed to detect expression of collagen type I alpha 1 chain (Col1a1), collagen type II alpha 1 chain (Col2a1), and collagen type III alpha 1 chain (Col3a1) in a 7500 thermal cycler (Applied Biosystems) using forward and reverse primers (Col1a1 forward 5′-GCATGGCCAAGAAGACATCC-3′; Col1a1 reverse 5′-CCTCGGGTTTCCACGTCTC-3′; Col2a1 forward 5′-AGAACAGCATCGCCTACCTG-3′; Col2a1 reverse 5′-CTTGCCCCACTTACCAGTGT-3′; Col3a1 forward 5′-TCAAGTCTGGAGTGGGAGG-3′; Col3a1 reverse 5′-TCCAGGATGTCCAGAAGAACCA-3′) and Fast SYBR Green PCR Master Mix (Applied Biosystems). Each sample was run in triplicate and

normalized to GAPDH followed by normalization to respective collagen content of *Acvr1*$^{+/+}$ on day 1.

Statistical analysis

Results are presented as the mean ± SEM. Paired or unpaired data sets were analyzed using two-tailed Student's *t* test or analysis of variance (ANOVA) (Bonferroni or Tukey–Kramer post-hoc test; one-way or two-way) to determine significance. Differences were considered statistically significant at $p < 0.05$. Significance and sample size (*n* for number in group or *N* for total sample size) are shown for each data set in the figure legends.

Study approval

All procedures were reviewed and approved by the Institutional Animal Care and Use Committee at the University of Pennsylvania.

ACKNOWLEDGMENTS

This work was supported by a National Institute of Arthritis and Musculoskeletal and Skin Diseases (NIAMS) Building Interdisciplinary Research Teams (BIRT) Award (E.M.S. and R.L.M.) from the National Institutes of Health (NIH) (3R01-AR041916-15S1). Additional support was provided by NIH Grants R01-AR071399 (E.M.S./R.L.M.) and R01-EB008722 (R.L.M.), the International Fibrodysplasia Ossificans Progressiva Association, the Center for Research in FOP and Related Disorders, the Ian Cali Endowment for FOP Research, the Whitney Weldon Endowment for FOP Research, the Cali-Weldon Professorship of FOP Research (E.M.S.), NIH NIAMS F31 AR069982-01A1 (A.S.), and National Science Foundation Graduate Research Fellowship DGE-0822 (C.M.M.). Histological and mechanical testing core facility resources were through the Penn Center for Musculoskeletal Disorders (P30 AR069619). We thank Deyu Zhang, Salin Chakkalakal, and Michael Convente for technical support for in vivo experiments. Additionally, we thank members of the "FOP laboratory" and the "Mauck laboratory" at the McKay Orthopaedic Research Laboratory for valuable comments and discussion.

REFERENCES

Achterberg VF, Buscemi L, Diekmann H, Smith-Clerc J, Schwengler H, Meister JJ, Wenck H, Gallinat S, Hinz B (2014). The nano-scale mechanical properties of the extracellular matrix regulate dermal fibroblast function. J Invest Dermatol 134, 1862–1872.

Almalki SG, Agrawal DK (2016). Key transcription factors in the differentiation of mesenchymal stem cells. Differentiation 92, 41–51.

Aratyn-Schaus Y, Oakes PW, Stricker J, Winter SP, Gardel ML (2010). Preparation of complaint matrices for quantifying cellular contraction. J Vis Exp 2010, 2173.

Arnsdorf EJ, Tummala P, Kwon RY, Jacobs CR (2009). Mechanically induced osteogenic differentiation–the role of RhoA, ROCKII and cytoskeletal dynamics. J Cell Sci 122(Pt 4), 546–553.

Bei Y, Hua-Huy T, Duong-Quy S, Nguyen VH, Chen W, Nicco C, Batteux F, Dinh-Xuan AT (2013). Long-term treatment with fasudil improves bleomycin-induced pulmonary fibrosis and pulmonary hypertension via inhibition of Smad2/3 phosphorylation. Pulm Pharmacol Ther 26, 635–643.

Bell DM, Leung KK, Wheatley SC, Ng LJ, Zhou S, Ling KW, Sham MH, Koopman P, Tam PP, Cheah KS (1997). SOX9 directly regulates the type-II collagen gene. Nat Genet 16, 174–178.

Billings PC, Fiori JL, Bentwood JL, O'Connell MP, Jiao X, Nussbaum B, Caron RJ, Shore EM, Kaplan FS (2008). Dysregulated BMP signaling and enhanced osteogenic differentiation of connective tissue progenitor cells from patients with fibrodysplasia ossificans progressiva (FOP). J Bone Miner Res 23, 305–313.

Brown AC, Fiore VF, Sulchek TA, Barker TH (2013). Physical and chemical microenvironmental cues orthogonally control the degree and duration of fibrosis-associated epithelial-to-mesenchymal transitions. J Pathol 229, 25–35.

Burg MA, Tillet E, Timpl R, Stallcup WB (1996). Binding of the NG2 proteoglycan to type VI collagen and other extracellular matrix molecules. J Biol Chem 271, 26110–26116.

Butcher DT, Alliston T, Weaver VM (2009). A tense situation: forcing tumour progression. Nat Rev Cancer 9, 108–122.

Carroll EP, Janicki JS, Pick R, Weber KT (1989). Myocardial stiffness and reparative fibrosis following coronary embolisation in the rat. Cardiovasc Res 23, 655–661.

Chakkalakal SA, Uchibe K, Convente MR, Zhang D, Economides AN, Kaplan FS, Pacifici M, Iwamoto M, Shore EM (2016). Palovarotene inhibits heterotopic ossification and maintains limb mobility and growth in mice with the human ACVR1 fibrodysplasia ossificans progressiva (FOP) mutation. J Bone Miner Res 31, 1666–1675.

Chakkalakal SA, Zhang D, Culbert AL, Convente MR, Caron RJ, Wright AC, Maidment AD, Kaplan FS, Shore EM (2012). An Acvr1 R206H knock-in mouse has fibrodysplasia ossificans progressiva. J Bone Miner Res 27, 1746–1756.

Chanet S, Martin AC (2014). Mechanical force sensing in tissues. Prog Mol Biol Transl Sci 126, 317–352.

Charge SB, Rudnicki MA (2004). Cellular and molecular regulation of muscle regeneration. Physiol Rev 84, 209–238.

Chen H, Ghori-Javed FY, Rashid H, Adhami MD, Serra R, Gutierrez SE, Javed A (2014). Runx2 regulates endochondral ossification through control of chondrocyte proliferation and differentiation. J Bone Miner Res 29, 2653–2665.

Chen X, Nadiarynkh O, Plotnikov S, Campagnola PJ (2012). Second harmonic generation microscopy for quantitative analysis of collagen fibrillar structure. Nat Protoc 7, 654–669.

Contreras O, Rebolledo DL, Oyarzun JE, Olguin HC, Brandan E (2016). Connective tissue cells expressing fibro/adipogenic progenitor markers increase under chronic damage: relevance in fibroblast-myofibroblast differentiation and skeletal muscle fibrosis. Cell Tissue Res 364, 647–660.

Convente MR, Chakkalakal SA, Yang E, Caron RJ, Zhang D, Kambayashi T, Kaplan FS, Shore EM (2018). Depletion of mast cells and macrophages impairs heterotopic ossification in an Acvr1(R206H) mouse model of Fibrodysplasia Ossificans Progressiva. J Bone Miner Res 33, 269–282.

Cosgrove BD, Mui KL, Driscoll TP, Caliari SR, Mehta KD, Assoian RK, Burdick JA, Mauck RL (2016). N-cadherin adhesive interactions modulate matrix mechanosensing and fate commitment of mesenchymal stem cells. Nat Mater 15, 1297–1306.

Couteaux R, Mira JC, d'Albis A (1988). Regeneration of muscles after cardiotoxin injury. I. Cytological aspects. Biol Cell 62, 171–182.

Cox TR, Erler JT (2011). Remodeling and homeostasis of the extracellular matrix: implications for fibrotic diseases and cancer. Dis Model Mech 4, 165–178.

Culbert AL, Chakkalakal SA, Theosmy EG, Brennan TA, Kaplan FS, Shore EM (2014). Alk2 regulates early chondrogenic fate in fibrodysplasia ossificans progressiva heterotopic endochondral ossification. Stem Cells 32, 1289–1300.

Czerwinska AM, Streminska W, Ciemerych MA, Grabowska I (2012). Mouse gastrocnemius muscle regeneration after mechanical or cardiotoxin injury. Folia Histochem Cytobiol 50, 144–153.

Dahl KN, Ribeiro AJ, Lammerding J (2008). Nuclear shape, mechanics, and mechanotransduction. Circ Res 102, 1307–1318.

Derynck R, Zhang YE (2003). Smad-dependent and Smad-independent pathways in TGF-beta family signalling. Nature 425, 577–584.

DesMarais V, Ghosh M, Eddy R, Condeelis J (2005). Cofilin takes the lead. J Cell Sci 118(Pt 1), 19–26.

Dingal PC, Bradshaw AM, Cho S, Raab M, Buxboim A, Swift J, Discher DE (2015). Fractal heterogeneity in minimal matrix models of scars modulates stiff-niche stem-cell responses via nuclear exit of a mechanorepressor. Nat Mater 14, 951–960.

Discher DE, Smith L, Cho S, Colasurdo M, Garcia AJ, Safran S (2017). Matrix mechanosensing: from scaling concepts in 'Omics data to mechanisms in the nucleus, regeneration, and cancer. Annu Rev Biophys 46, 295–315.

Du J, Chen X, Liang X, Zhang G, Xu J, He L, Zhan Q, Feng XQ, Chien S, Yang C (2011). Integrin activation and internalization on soft ECM as a mechanism of induction of stem cell differentiation by ECM elasticity. Proc Natl Acad Sci USA 108, 9466–9471.

Ducy P, Zhang R, Geoffroy V, Ridall AL, Karsenty G (1997). Osf2/Cbfa1: a transcriptional activator of osteoblast differentiation. Cell 89, 747–754.

Engler AJ, Sen S, Sweeney HL, Discher DE (2006). Matrix elasticity directs stem cell lineage specification. Cell 126, 677–689.

Fehlings MG, Theodore N, Harrop J, Maurais G, Kuntz C, Shaffrey CI, Kwon BK, Chapman J, Yee A, Tighe A, McKerracher L (2011). A phase I/IIa clinical trial of a recombinant Rho protein antagonist in acute spinal cord injury. J Neurotrauma 28, 787–796.

Fukuda T, Kohda M, Kanomata K, Nojima J, Nakamura A, Kamizono J, Noguchi Y, Iwakiri K, Kondo T, Kurose J, *et al*. (2009). Constitutively activated ALK2 and increased SMAD1/5 cooperatively induce bone morphogenetic protein signaling in fibrodysplasia ossificans progressiva. J Biol Chem 284, 7149–7156.

Garreta E, Genove E, Borros S, Semino CE (2006). Osteogenic differentiation of mouse embryonic stem cells and mouse embryonic fibroblasts in a three-dimensional self-assembling peptide scaffold. Tissue Eng 12, 2215–2227.

Georges PC, Miller WJ, Meaney DF, Sawyer ES, Janmey PA (2006). Matrices with compliance comparable to that of brain tissue select neuronal over glial growth in mixed cortical cultures. Biophys J 90, 3012–3018.

Guilak F, Cohen DM, Estes BT, Gimble JM, Liedtke W, Chen CS (2009). Control of stem cell fate by physical interactions with the extracellular matrix. Cell Stem Cell 5, 17–26.

Han WM, Heo SJ, Driscoll TP, Delucca JF, McLeod CM, Smith LJ, Duncan RL, Mauck RL, Elliott DM (2016). Microstructural heterogeneity directs micromechanics and mechanobiology in native and engineered fibrocartilage. Nat Mater 15, 477–484.

Hatsell SJ, Idone V, Wolken DM, Huang L, Kim HJ, Wang L, Wen X, Nannuru KC, Jimenez J, Xie L, *et al*. (2015). ACVR1R206H receptor mutation causes fibrodysplasia ossificans progressiva by imparting responsiveness to activin A. Sci Transl Med 7, 303ra137.

Haupt J, Deichsel A, Stange K, Ast C, Bocciardi R, Ravazzolo R, Di Rocco M, Ferrari P, Landi A, Kaplan FS, *et al*. (2014). ACVR1 p.Q207E causes classic fibrodysplasia ossificans progressiva and is functionally distinct from the engineered constitutively active ACVR1 p.Q207D variant. Hum Mol Genet 23, 5364–5377.

Hay E, Lemonnier J, Fromigue O, Marie PJ (2001). Bone morphogenetic protein-2 promotes osteoblast apoptosis through a Smad-independent, protein kinase C-dependent signaling pathway. J Biol Chem 276, 29028–29036.

Heo SJ, Han WM, Szczesny SE, Cosgrove BD, Elliott DM, Lee DA, Duncan RL, Mauck RL (2016). Mechanically induced chromatin condensation requires cellular contractility in mesenchymal stem cells. Biophys J 111, 864–874.

Heo SJ, Thorpe SD, Driscoll TP, Duncan RL, Lee DA, Mauck RL (2015). Biophysical regulation of chromatin architecture instills a mechanical memory in mesenchymal stem cells. Sci Rep 5, 16895.

Hinz B (2007). Formation and function of the myofibroblast during tissue repair. J Invest Dermatol 127, 526–537.

Hinz B (2010). The myofibroblast: paradigm for a mechanically active cell. J Biomech 43, 146–155.

Hinz B, Phan SH, Thannickal VJ, Prunotto M, Desmouliere A, Varga J, De Wever O, Mareel M, Gabbiani G (2012). Recent developments in myofibroblast biology: paradigms for connective tissue remodeling. Am J Pathol 180, 1340–1355.

Ingber DE (2003). Mechanobiology and diseases of mechanotransduction. Ann Med 35, 564–577.

Irianto J, Pfeifer CR, Xia Y, Discher DE (2016). SnapShot: mechanosensing matrix. Cell 165, 1820–1820.e1821.

Ivanovska IL, Swift J, Spinler K, Dingal D, Cho S, Discher DE (2017). Cross-linked matrix rigidity and soluble retinoids synergize in nuclear lamina regulation of stem cell differentiation. Mol Biol Cell 28, 2010–2022.

Jain RK, Martin JD, Stylianopoulos T (2014). The role of mechanical forces in tumor growth and therapy. Annu Rev Biomed Eng 16, 321–346.

Jazayeri M, Shokrgozar MA, Haghighipour N, Mahdian R, Farrokhi M, Bonakdar S, Mirahmadi F, Abbariki TN (2015). Evaluation of mechanical and chemical stimulations on osteocalcin and Runx2 expression in mesenchymal stem cells. Mol Cell Biomech 12, 197–213.

Kai F, Laklai H, Weaver VM (2016). Force matters: biomechanical regulation of cell invasion and migration in disease. Trends Cell Biol 26, 486–497.

Kaplan FS, Le Merrer M, Glaser DL, Pignolo RJ, Goldsby RE, Kitterman JA, Groppe J, Shore EM (2008). Fibrodysplasia ossificans progressiva. Best Pract Res Clin Rheumatol 22, 191–205.

Kaplan FS, Tabas JA, Gannon FH, Finkel G, Hahn GV, Zasloff MA (1993). The histopathology of fibrodysplasia ossificans progressiva. An endochondral process. J Bone Joint Surg Am 75, 220–230.

Kaplan FS, Xu M, Seemann P, Connor JM, Glaser DL, Carroll L, Delai P, Fastnacht-Urban E, Forman SJ, Gillessen-Kaesbach G, *et al*. (2009). Classic and atypical fibrodysplasia ossificans progressiva (FOP) phenotypes are caused by mutations in the bone morphogenetic protein (BMP) type I receptor ACVR1. Hum Mutat 30, 379–390.

Klingberg F, Hinz B, White ES (2013). The myofibroblast matrix: implications for tissue repair and fibrosis. J Pathol 229, 298–309.

Knipe RS, Tager AM, Liao JK (2015). The Rho kinases: critical mediators of multiple profibrotic processes and rational targets for new therapies for pulmonary fibrosis. Pharmacol Rev 67, 103–117.

Kobayashi H, Gao Y, Ueta C, Yamaguchi A, Komori T (2000). Multilineage differentiation of Cbfa1-deficient calvarial cells in vitro. Biochem Biophys Res Commun 273, 630–636.

Komori T, Yagi H, Nomura S, Yamaguchi A, Sasaki K, Deguchi K, Shimizu Y, Bronson RT, Gao YH, Inada M, *et al*. (1997). Targeted disruption of Cbfa1 results in a complete lack of bone formation owing to maturational arrest of osteoblasts. Cell 89, 755–764.

Kopf J, Paarmann P, Hiepen C, Horbelt D, Knaus P (2014). BMP growth factor signaling in a biomechanical context. Biofactors 40, 171–187.

Lees-Shepard JB, Yamamoto M, Biswas AA, Stoessel SJ, Nicholas SE, Cogswell CA, Devarakonda PM, Schneider MJ Jr, Cummins SM, Legendre NP, *et al*. (2018). Activin-dependent signaling in fibro/adipogenic progenitors causes fibrodysplasia ossificans progressiva. Nat Commun 9, 471.

Lengner CJ, Lepper C, van Wijnen AJ, Stein JL, Stein GS, Lian JB (2004). Primary mouse embryonic fibroblasts: a model of mesenchymal cartilage formation. J Cell Physiol 200, 327–333.

Lessey EC, Guilluy C, Burridge K (2012). From mechanical force to RhoA activation. Biochemistry 51, 7420–7432.

Levental I, Levental KR, Klein EA, Assoian R, Miller RT, Wells RG, Janmey PA (2010). A simple indentation device for measuring micrometer-scale tissue stiffness. J Phys Condens Matter 22, 194120.

Liao JK, Seto M, Noma K (2007). Rho kinase (ROCK) inhibitors. J Cardiovasc Pharmacol 50, 17–24.

Liu S, Xu SW, Blumbach K, Eastwood M, Denton CP, Eckes B, Krieg T, Abraham DJ, Leask A (2010). Expression of integrin beta1 by fibroblasts is required for tissue repair in vivo. J Cell Sci 123(Pt 21), 3674–3682.

Majd SE, Kuijer R, Kowitsch A, Groth T, Schmidt TA, Sharma PK (2014). Both hyaluronan and collagen type II keep proteoglycan 4 (lubricin) at the cartilage surface in a condition that provides low friction during boundary lubrication. Langmuir 30, 14566–14572.

Maruthamuthu V, Sabass B, Schwarz US, Gardel ML (2011). Cell-ECM traction force modulates endogenous tension at cell-cell contacts. Proc Natl Acad Sci USA 108, 4708–4713.

Matsubara T, Kida K, Yamaguchi A, Hata K, Ichida F, Meguro H, Aburatani H, Nishimura R, Yoneda T (2008). BMP2 regulates Osterix through Msx2 and Runx2 during osteoblast differentiation. J Biol Chem 283, 29119–29125.

McCarthy EF, Sundaram M (2005). Heterotopic ossification: a review. Skeletal Radiol 34, 609–619.

Ng LJ, Wheatley S, Muscat GE, Conway-Campbell J, Bowles J, Wright E, Bell DM, Tam PP, Cheah KS, Koopman P (1997). SOX9 binds DNA, activates transcription, and coexpresses with type II collagen during chondrogenesis in the mouse. Dev Biol 183, 108–121.

Olsen DR, Peltonen J, Jaakkola S, Chu ML, Uitto J (1989). Collagen gene expression by cultured human skin fibroblasts. Abundant steady-state levels of type VI procollagen messenger RNAs. J Clin Invest 83, 791–795.

Otto F, Thornell AP, Crompton T, Denzel A, Gilmour KC, Rosewell IR, Stamp GW, Beddington RS, Mundlos S, Olsen BR, *et al*. (1997). Cbfa1, a candidate gene for cleidocranial dysplasia syndrome, is essential for osteoblast differentiation and bone development. Cell 89, 765–771.

Pignolo RJ, Foley KL (2005). Nonhereditary heterotopic ossification. Implications for injury, arthropathy, and aging. Clin Rev Bone Miner Metab 3, 261–266.

Rahman MS, Akhtar N, Jamil HM, Banik RS, Asaduzzaman SM (2015). TGF-beta/BMP signaling and other molecular events: regulation of osteoblastogenesis and bone formation. Bone Res 3, 15005.

Raub CB, Putnam AJ, Tromberg BJ, George SC (2010). Predicting bulk mechanical properties of cellularized collagen gels using multiphoton microscopy. Acta Biomater 6, 4657–4665.

Reddi AH (2000). Morphogenetic messages are in the extracellular matrix: biotechnology from bench to bedside. Biochem Soc Trans 28, 345–349.

Riento K, Ridley AJ (2003). Rocks: multifunctional kinases in cell behaviour. Nat Rev Mol Cell Biol 4, 446–456.

Roduit C, Sekatski S, Dietler G, Catsicas S, Lafont F, Kasas S (2009). Stiffness tomography by atomic force microscopy. Biophys J 97, 674–677.

Roeder BA, Kokini K, Sturgis JE, Robinson JP, Voytik-Harbin SL (2002). Tensile mechanical properties of three-dimensional type I collagen extracellular matrices with varied microstructure. J Biomech Eng 124, 214–222.

Saeed H, Taipaleenmaki H, Aldahmash AM, Abdallah BM, Kassem M (2012). Mouse embryonic fibroblasts (MEF) exhibit a similar but not identical

phenotype to bone marrow stromal stem cells (BMSC). Stem Cell Rev 8, 318–328.
Salazar VS, Gamer LW, Rosen V (2016). BMP signalling in skeletal development, disease and repair. Nat Rev Endocrinol 12, 203–221.
Shen Q, Little SC, Xu M, Haupt J, Ast C, Katagiri T, Mundlos S, Seemann P, Kaplan FS, Mullins MC, Shore EM (2009). The fibrodysplasia ossificans progressiva R206H ACVR1 mutation activates BMP-independent chondrogenesis and zebrafish embryo ventralization. J Clin Invest 119, 3462–3472.
Shimizu Y, Dobashi K, Iizuka K, Horie T, Suzuki K, Tukagoshi H, Nakazawa T, Nakazato Y, Mori M (2001). Contribution of small GTPase Rho and its target protein rock in a murine model of lung fibrosis. Am J Respir Crit Care Med 163, 210–217.
Shore EM (2012). Fibrodysplasia ossificans progressiva: a human genetic disorder of extraskeletal bone formation, or—how does one tissue become another? Wiley Interdiscip Rev Dev Biol 1, 153–165.
Shore EM, Kaplan FS (2010). Inherited human diseases of heterotopic bone formation. Nat Rev Rheumatol 6, 518–527.
Shore EM, Xu M, Feldman GJ, Fenstermacher DA, Cho TJ, Choi IH, Connor JM, Delai P, Glaser DL, LeMerrer M, *et al*. (2006). A recurrent mutation in the BMP type I receptor ACVR1 causes inherited and sporadic fibrodysplasia ossificans progressiva. Nat Genet 38, 525–527.
Smith L, Cho S, Discher DE (2017). Mechanosensing of matrix by stem cells: From matrix heterogeneity, contractility, and the nucleus in pore-migration to cardiogenesis and muscle stem cells in vivo. Semin Cell Dev Biol 71, 84–98.
Smith LR, Cho S, Discher DE (2018). Stem cell differentiation is regulated by extracellular matrix mechanics. Physiology (Bethesda) 33, 16–25.
Sun J, Li J, Li C, Yu Y (2015). Role of bone morphogenetic protein-2 in osteogenic differentiation of mesenchymal stem cells. Mol Med Rep 12, 4230–4237.
Swift J, Ivanovska IL, Buxboim A, Harada T, Dingal PC, Pinter J, Pajerowski JD, Spinler KR, Shin JW, Tewari M, *et al*. (2013). Nuclear lamin-A scales with tissue stiffness and enhances matrix-directed differentiation. Science 341, 1240104.
Tee SY, Fu J, Chen CS, Janmey PA (2011). Cell shape and substrate rigidity both regulate cell stiffness. Biophys J 100, L25–L27.
Thomas G, Burnham NA, Camesano TA, Wen Q (2013). Measuring the mechanical properties of living cells using atomic force microscopy. J Vis Exp 2013, DOI: 10.3791/50497.
Thomas K, Engler AJ, Meyer GA (2014). Extracellular matrix regulation in the muscle satellite cell niche. Connect Tissue Res 56, 1–8.
Tzima E (2006). Role of small GTPases in endothelial cytoskeletal dynamics and the shear stress response. Circ Res 98, 176–185.
van Dinther M, Visser N, de Gorter DJ, Doorn J, Goumans MJ, de Boer J, ten Dijke P (2010). ALK2 R206H mutation linked to fibrodysplasia ossificans progressiva confers constitutive activity to the BMP type I receptor and sensitizes mesenchymal cells to BMP-induced osteoblast differentiation and bone formation. J Bone Miner Res 25, 1208–1215.
Versaevel M, Grevesse T, Gabriele S (2012). Spatial coordination between cell and nuclear shape within micropatterned endothelial cells. Nat Commun 3, 671.
Vignaud A, Hourde C, Torres S, Caruelle JP, Martelly I, Keller A, Ferry A (2005). Functional, cellular and molecular aspects of skeletal muscle recovery after injury induced by snake venom from Notechis scutatus scutatus. Toxicon 45, 789–801.
Wang RN, Green J, Wang Z, Deng Y, Qiao M, Peabody M, Zhang Q, Ye J, Yan Z, Denduluri S, *et al*. (2014). Bone Morphogenetic Protein (BMP) signaling in development and human diseases. Genes Dis 1, 87–105.
Wang Y, Belflower RM, Dong YF, Schwarz EM, O'Keefe RJ, Drissi H (2005). Runx1/AML1/Cbfa2 mediates onset of mesenchymal cell differentiation toward chondrogenesis. J Bone Miner Res 20, 1624–1636.
Wang YK, Yu X, Cohen DM, Wozniak MA, Yang MT, Gao L, Eyckmans J, Chen CS (2012). Bone morphogenetic protein-2-induced signaling and osteogenesis is regulated by cell shape, RhoA/ROCK, and cytoskeletal tension. Stem Cells Dev 21, 1176–1186.
Watsky MA, Weber KT, Sun Y, Postlethwaite A (2010). New insights into the mechanism of fibroblast to myofibroblast transformation and associated pathologies. Int Rev Cell Mol Biol 282, 165–192.
Wells RG (2008). The role of matrix stiffness in regulating cell behavior. Hepatology 47(4), 1394–1400.
Wipff PJ, Rifkin DB, Meister JJ, Hinz B (2007). Myofibroblast contraction activates latent TGF-beta1 from the extracellular matrix. J Cell Biol 179, 1311–1323.
Xiao G, Jiang D, Thomas P, Benson MD, Guan K, Karsenty G, Franceschi RT (2000). MAPK pathways activate and phosphorylate the osteoblast-specific transcription factor, Cbfa1. J Biol Chem 275, 4453–4459.
Yang C, Tibbitt MW, Basta L, Anseth KS (2014). Mechanical memory and dosing influence stem cell fate. Nat Mater 13, 645–652.
Young JL, Kretchmer K, Ondeck MG, Zambon AC, Engler AJ (2014). Mechanosensitive kinases regulate stiffness-induced cardiomyocyte maturation. Sci Rep 4, 6425.
Zhang P, Wu Y, Jiang Z, Jiang L, Fang B (2012). Osteogenic response of mesenchymal stem cells to continuous mechanical strain is dependent on ERK1/2-Runx2 signaling. Int J Mol Med 29, 1083–1089.
Zhou Y, Huang X, Hecker L, Kurundkar D, Kurundkar A, Liu H, Jin TH, Desai L, Bernard K, Thannickal VJ (2013). Inhibition of mechanosensitive signaling in myofibroblasts ameliorates experimental pulmonary fibrosis. J Clin Invest 123, 1096–1108.